Tomographic PIV and pressure reconstructions on a drone wing vortex

Nathaniel T. Baker, Marco Carini, Philippe Cornic, Cédric Illoul, Benjamin Leclaire, Gilles Losfeld, Jean-Claude Monnier, Vianney Nowinski, Christophe Verbeke

13th International Symposium on Particle Image Velocimetry – ISPIV 2019
Munich, Germany, July 22-24, 2019

Tomographic PIV and pressure reconstructions on a drone wing vortex

Nathaniel T. Baker[1*], Marco Carini[1], Philippe Cornic[2], Cédric Illoul[1], Benjamin Leclaire[1], Gilles Losfeld[1], Jean-Claude Monnier[3], Vianney Nowinski[3], Christophe Verbeke[3]

[1] ONERA/DAAA, Université Paris-Saclay, F-92190 Meudon, France

[2] ONERA/DTIS, Université Paris-Saclay, F-91123 Palaiseau, France

[3] ONERA/DAAA, Laboratoire de Mcanique des Fluides de Lille - Kampé de Fériet, F-59045 Lille, France

[*] nathaniel.baker@onera.fr

Abstract

We present the results of a Tomographic PIV campaign investigating the wingtip vortex over a drone upper surface at high angle of attack, together with associated three-dimensional pressure reconstructions. Our final aim is to assess the accuracy of a newly introduced pressure from TomoPIV method, the Pressure Schur Complement (Carini et al. ISPIV 2019), in realistic and difficult experimental conditions. The model is set at 20^o angle of attack in order to obtain a strong vortex. Measurements in a volume encompassing a wall pressure tap generatrix, used for comparison, are performed both in natural conditions and with jet blowing at the leading edge. While a strong vortex is indeed observed in the former case, leading edge blowing is observed to lead to vortex breakdown, with a dramatic core widening and a higher turbulence intensity. PSC reconstruction in the natural case captures truthfully the pressure drop due to the vortex, except in a flow zone of reduced extent located directly below it. In the case with blowing however, a large discrepancy with the wall pressure taps is observed. Both these limitations are presently ascribed to the existence of a gap between the closest TomoPIV measurement location and the wall, within which the pressure might significantly change due to streamline curvature induced by vorticity.

1 Introduction

Pressure from Tomographic PIV (TomoPIV) has received important attention over the last decade, as a result of its potential to provide an important wealth of measurements in a single operation (i.e. velocity and pressure fields, wall pressures, and possibly forces). As identified by e.g. Van Gent et al. (2017), the choice of adapted boundary conditions, and formulation of algorithms leading to tractable computational times, remain some of the important research topics in the field. In order to assess a newly introduced pressure from TomoPIV method, the Pressure Schur Complement (see our companion paper Carini et al.), we performed dedicated experiments in a the semi-industrial wind-tunnel L1, at ONERA Lille centre. We considered a flying wing model of the generic SACCON geometry, which has been the subject of a series of research studies in recent years (see for instance Schütte et al., 2012) and is known to exhibit complex vortical structures on its upper surface. Tomographic PIV was performed in a volumic zone embedding a generatrix of wall pressure taps, that were used for comparison, both in natural flow conditions and with leading edge control by fluidic actuation (continuous blowing). The aim of this paper is to present in detail the characteristics of the experimental setup and results, as well as the flow fields obtained in both cases. Then, mean pressure fields yielded by the PSC method on the mean flow fields (using the Reynolds-Averaged Navier-Stokes equations) will be examined, and compared with the pressure measurements at the wall. Finally, conclusions and possible next steps of this work will be presented.

2 Experimental setup

2.1 Model and aerodynamic conditions

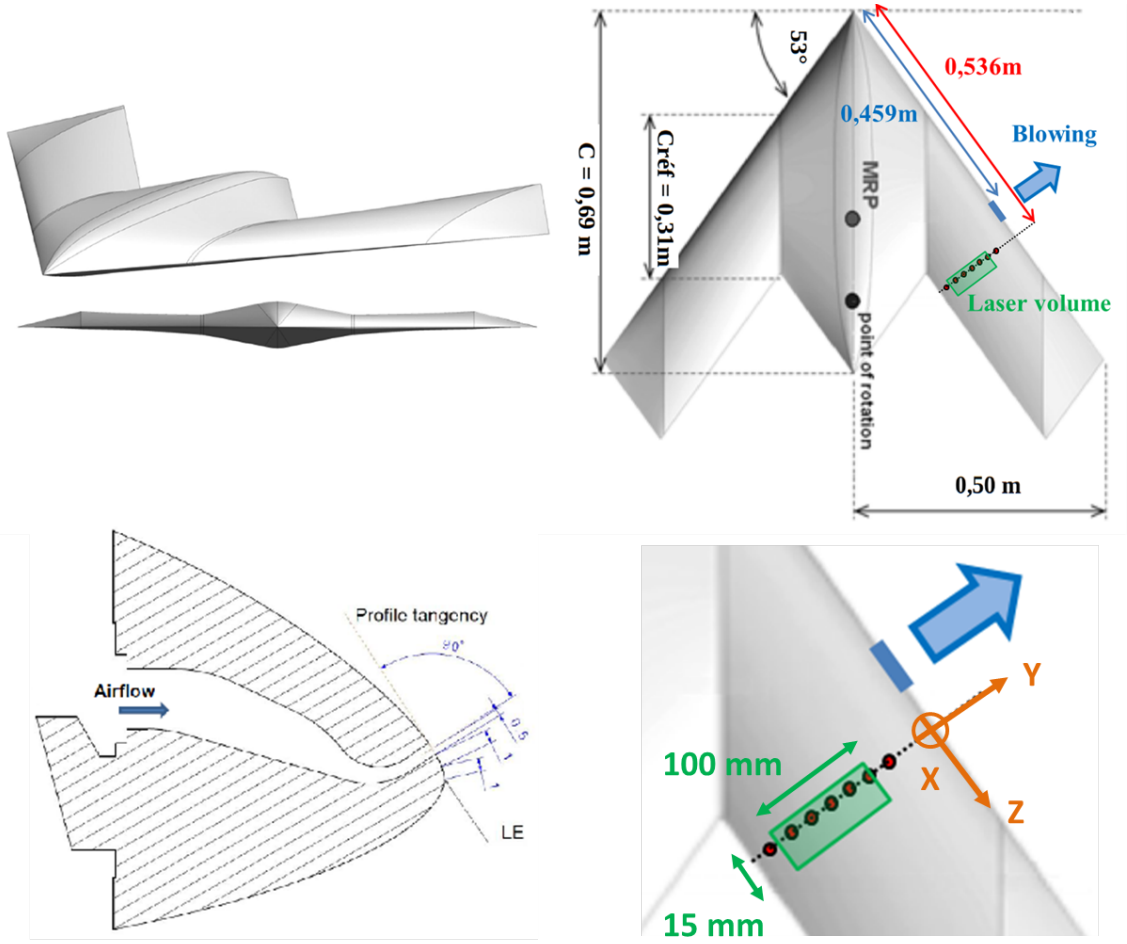

Figure 1: Schematic of the SACCON model. Top: planform and geometric parameters. Bottom: left: leading edge (LE) blowing design sketch, right: close-up on the zone measured by TomoPIV, featuring the volume illumination (green) and wall pressure taps (red dots), as well as the frame of reference used for the results.

The drone model considered here is the SACCON generic geometry, which has been the subject of several recent studies (see for instance Schütte et al., 2012; Tormalm et al., 2016). It is known to exhibit complex vortical structures on its upper surface as the angle of attack is increased, possibly leading to manoeuverability issues such as pitching moment crisis or vortex breakdown. It has therefore received attention in the framework of flow control strategies, in particular using fluidic actuation (see, e.g. Jentzsch et al., 2016). As can be seen in Figure 1, it has a diamond shape and is characterized by a 53^o sweep angle. The model considered here has a $1m$ wingspan, with its chord $c_{ref} = 0.31m$ taken as reference for building dimensionless quantities. It is equipped with several lines of pressure taps. One of these, highlighted in Figure 1, has been singled out to choose the flow zone studied herein, from which pressure reconstruction from TomoPIV is performed, and will serve as a reference. As a strategy to mitigate pitching moment crisis observed at moderate angles of attack (see for instance Schütte et al., 2012), studies have proposed to perform leading-edge actuation via fluidic control. The present model is thus equipped with several slits located on its leading edges, from which continuous air blowing can be performed. As one of these slits has been shown to have maximum aerodynamic efficiency, we will consider it here as a way to drastically change flow conditions in the measured zone without changing the drone angle of attack. The slit is 1mm

wide and 50mm long, so that its downstream end is located 27mm upstream of the pressure tap generatrix (see figure 1).

Experiments have been performed in ONERA Lille's L1 low-speed wind tunnel, which has a $2.4m$ wide dodecagonal test section equipped with various optical accesses. Consistently with previous test campaigns, the free-stream velocity was fixed at $U_\infty = 35m.s^{-1}$, corresponding to a chord Reynolds number $Re_\infty = 1.1\,10^6$ and Mach number $Ma_\infty = U_\infty/\sqrt{\gamma r T_\infty} = 0.1$. The model's angle of attack was fixed at 20^o, at which the pressure signal of the singled out taps has been observed to span a wide dynamic range. In the literature, such an angle value is associated with the possibility of breakdown of the vortical structures on the model upper surface (Schütte et al., 2012; Le Roy et al., 2014). Two configurations have been considered in detail: in natural conditions, and with leading-edge blowing on. In the latter case, blowing mass flow rate was set to $9.8g.s^{-1}$, corresponding to an exhaust velocity of $100m.s^{-1}$.

In all this study, we will consider a frame of reference associated with the pressure tap generatrix, the wing leading edge and the measurement domain. As sketched in Figure 1 (bottom left), Z is aligned with the right leading edge, pointing downstream, Y is parallel to the pressure tap generatrix, and X is wall normal. The origin of the frame of reference is taken at the leading edge along the Y axis, so that Y coordinates of the taps are negative. Associated to these coordinates we define the respective velocity components, with mean and fluctuation decomposition, $(u,v,w) = (U+u', V+v', W+w')$.

2.2 Measurements

Due to the curved nature of the wing surface in the zone of interest (see in particular Figure 1 top left), it was not possible to consider volume illumination originating from a lateral direction. This would have led to occultations, leading to important gaps between the closest location of the TomoPIV measurements compared to the wall and the pressure taps. It has thus been decided to illuminate from above the wing. In order to mitigate as much as possible spurious light reflections in the images, the wing upper surface has been painted with Rhodamine. As the present kind of vortical flows can be very sensitive to roughness, it has been decided not to paint only the measured zone, but the whole upper wing surface.

Figure 2 shows the wing installed in the L1 wind-tunnel, set at 20^o angle of attack, with volume illumination on. Also shown in this figure are pictures of the illumination system, originating from above the test section, and of the four cameras. A Brillant B Quantel laser was used, with an energy of 400 mJ per pulse, together with a LaVision volume generator and a diaphragm to shape the resulting ellipsoid into a parallelepiped. As sketched in Figure 1, the laser volume, of useful thickness $15mm$, was placed parallel to the pressure tap line. Its mid-plane did not coincide with this line, and was instead shifted downstream, so that the pressure tap generatrix (coordinate $Z = 0$) is located $5mm$ downstream of it. This decision has been taken in order to minimize the extent of the near wall zone inaccessible to TomoPIV measurements due to remaining light reflections. Indeed, all four cameras (LaVision Imager ProX 4 Mpixel CCD cameras), were placed on the same side of the wind tunnel, as depicted in figure 2 (top right), and observing laterally or from downstream. Each of these cameras was equipped with a Scheimpflug mount and an $f = 200\ mm$ lens.

Tests were performed for both the natural and LE blowing cases using recording 2500 images at 5Hz, with an inter-frame time of 10μs. Pressure tap acquisition was done at the same frequency, with same number of samples.

3 TomoPIV processing and results

3.1 Processing parameters

Camera calibration was performed using a pinhole model, following an in-house procedure (Cornic et al., 2016), defining the reference plane (first image acquired and processed) to coincide with the wing wall-normal plane cutting the wing along the pressure tap generatrix. Note that the origin for the X axis is here kept as the centre of the calibration plate, as the wing upper surface is curved and does not correspond to a fixed value of X. During the tests, strong vibrations of the camera system have been observed. A first partial compensation has been found by supporting the $200mm$ lenses with rigid foam blocks. However, substantial vibrations remained, which imposed to perform self-calibration (also following the algorithm of Cornic et al., 2016), for each individual snapshot. Due to a quite low signal-to-noise ratio in the images (see sample images in Figure 3, where contrast has been strongly enhanced), the self-calibration was observed to converge on a part of the snapshots only. As a result, the useful number of samples for averaging considered so far is equal to 863 for the natural case, and 712 for the case with LE blowing on.

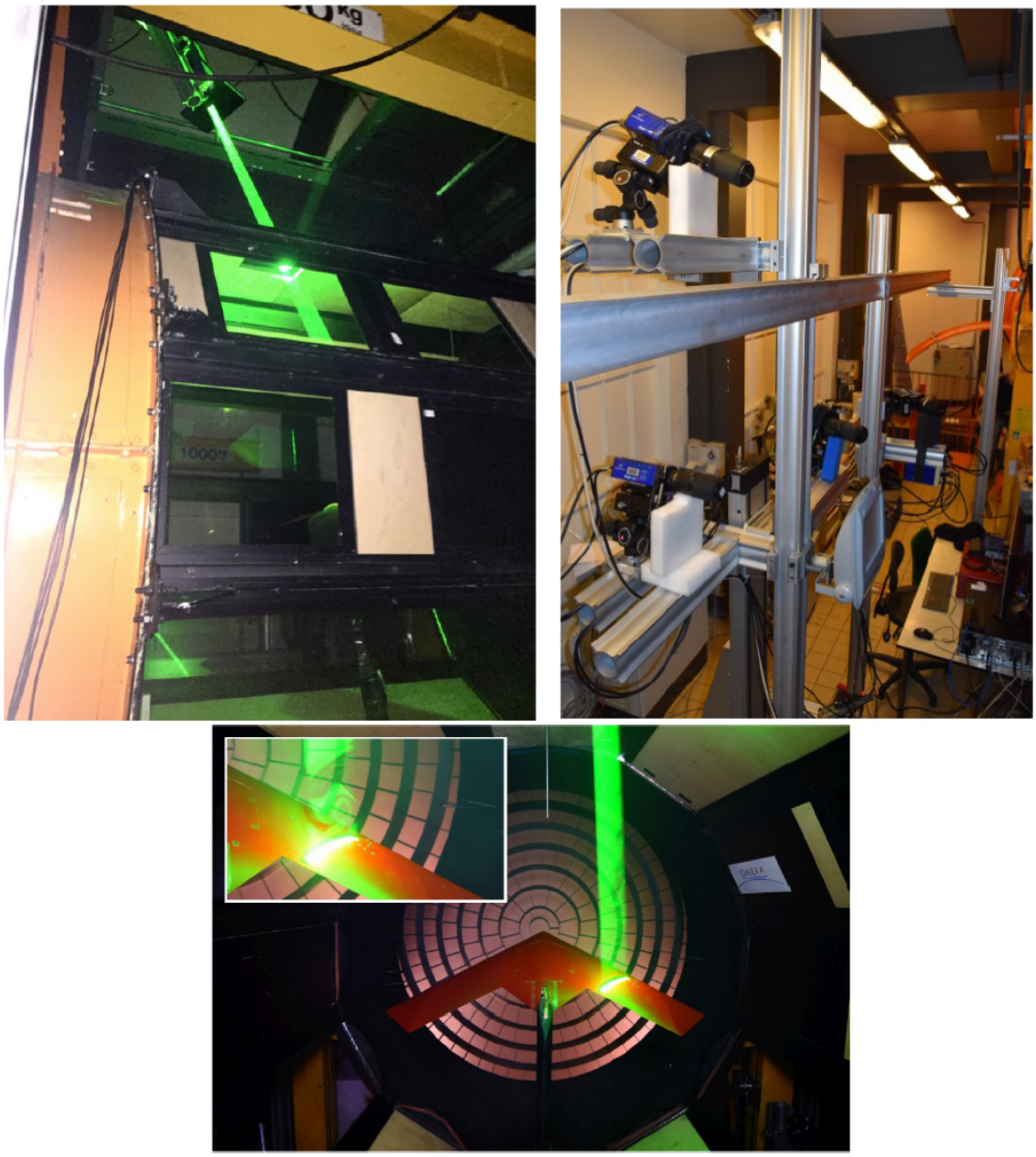

Figure 2: Elements of the experiment and of the tomographic PIV setup. Top left: volumic illumination, generated from above ONERA L1 wind-tunnel's test section. Top right: four camera system, installed roughly at 1.5m horizontally from the test section. Bottom: model with rhodamine painted upper surface installed in the test section, with volumic illumination on; the top-left inset shows a close-up on the measured volume, highlighting the vortical structure of the flow.

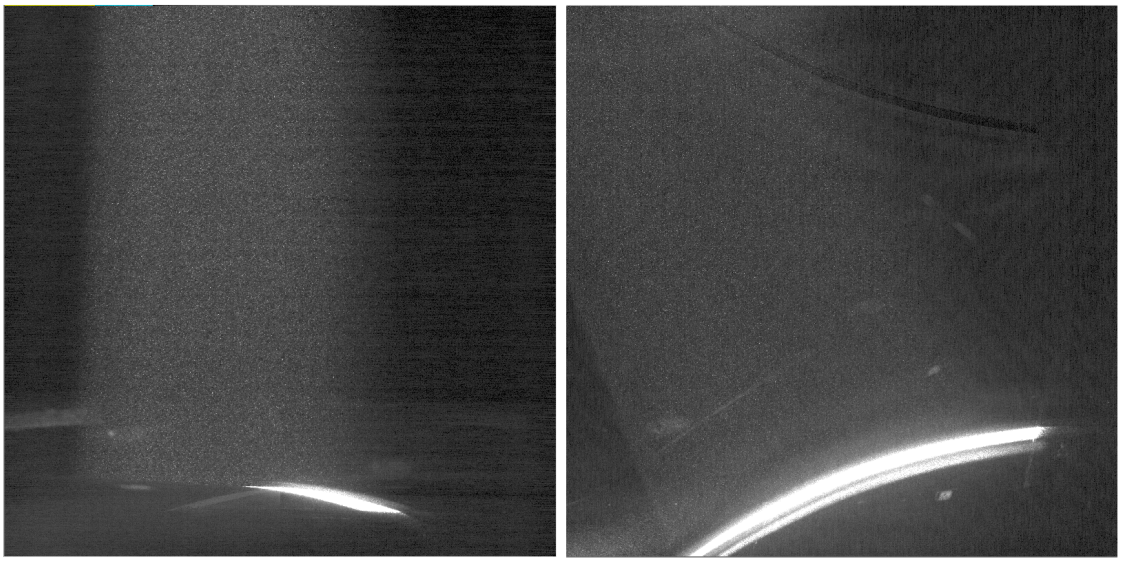

Figure 3: Sample images of two cameras for the run in natural conditions, featuring the remaining light reflection at the wall. Seeding density has been estimated to 0.05 particles per pixel.

As can be seen in Figure 3, Rhodamine paint could not prevent a strong light reflection at the wall, corresponding to the impact of the laser volume on the model. This led to use masking in the images, and to the existence of a gap between the highest location in X (closest to the wall) of the TomoPIV measurements and the model wall. Its exact magnitude has not been quantified yet and is the subject of future steps in the study. These will also account for vibrations of the model itself, which have been measured with model deformation measurement and evaluated to $\pm 0.3mm$. Aside from masking, standard pre-processing has been applied to the images, i.e. subtraction of historical minimum, and grey level rescaling in order to account for different signal-to-noise ratios among the cameras, probably due to different Mie scattering regimes.

Tomographic reconstruction has been performed with an in-house implementation of MLOS-SMART (Atkinson and Soria, 2009), using 25 iterations. With the present geometric setup, a voxel size of $72.9\mu m$ has been obtained. Reconstructed volumes have an extent of 80mm$\times$145mm$\times$15mm, corresponding to $1100 \times 1990 \times 206$ voxels. Three-dimensional correlation of the particle volumes with the FOLKI3D algorithm (Cheminet et al., 2014) has then yielded the flow snapshots. Interrogation volumes of $21 \times 21 \times 21$ voxels with Gaussian weighting have been considered, leading to a final spatial resolution estimated to $0.36mm$.

3.2 Analysis of the 3D flow fields

To analyse the volumic flow fields, we present, for each case, both three dimensional representations (Figures 4 and 5) and slices of the mean flow and Reynolds stresses at $Z = 0$ (Figures 6 and 7), corresponding to the location of the pressure tap generatrix on the wall model. As can be firstly observed in Figures 4 and 6, the flow in natural conditions is largely dominated by a strong vortex, located in the rightmost part (larger values of Y), closest to the leading edge. In Figure 4, the three-dimensional iso-contour $W = 5m.s^{-1}$ has been represented as a means to evidence the structure of this wingtip vortex within the volume, as iso-contours of W overall have a shape similar to that of the streamlines. Note, however, that the vortex core is located slightly below (at a slightly larger X value) compared to the location of minimum W. Also, while low values of W are observed close to the vortex core, they here remain strictly positive.

Upon comparing mean flows for both runs, it is clear that leading-edge blowing has a dramatic effect on the flow structure, leading in fact to vortex breakdown. Important negative W velocities are observed in the vortex core (note that Figure 5 also includes iso-contour $W = 0m.s^{-1}$), and streamlines clearly illustrate this internal flow reversal. Besides, as classically observed in situations of breakdown, the vortex core has considerably expanded, as can be seen by comparing the extents of isolines $W = 5m.s^{-1}$ for both runs. Another very apparent, and expected difference between the two cases is that the vortex with breakdown has a much smaller rotation velocity (which can be here evidenced through the levels of U and V in the slices of Figures 6 and 7). This is consistent with the dramatic widening of the vortex core due to breakdown, and is

a consequence of angular momentum or circulation conservation.

For both runs, the respective vortical structure is also quite cleary evidenced in the Reynolds stresses fields, as shown in Figures 6 and 7. In the natural case, where the vortex has a moderate size and is almost fully contained in the volume (except for its rightmost part, close to the leading edge), one clearly observes in each component an ellipsoidal organization of the contours, with one lobe on the diagonal terms $\langle u'^2 \rangle$, $\langle v'^2 \rangle$ and $\langle w'^2 \rangle$, and two lobes of opposite signs on the off-diagonal terms $\langle u'v' \rangle$, $\langle u'w' \rangle$ and $\langle v'w' \rangle$. Logically, in the case with leading edge blowing, Reynolds stresses all have larger amplitudes, consistent with the increase in turbulence induced by vortex breakdown, and spread over a much wider region, similar to the widening of the vortex core. For most of them, and contrary to the natural case, the observation field is now too small for these stresses to vanish, as the vortex no more entirely fits within it.

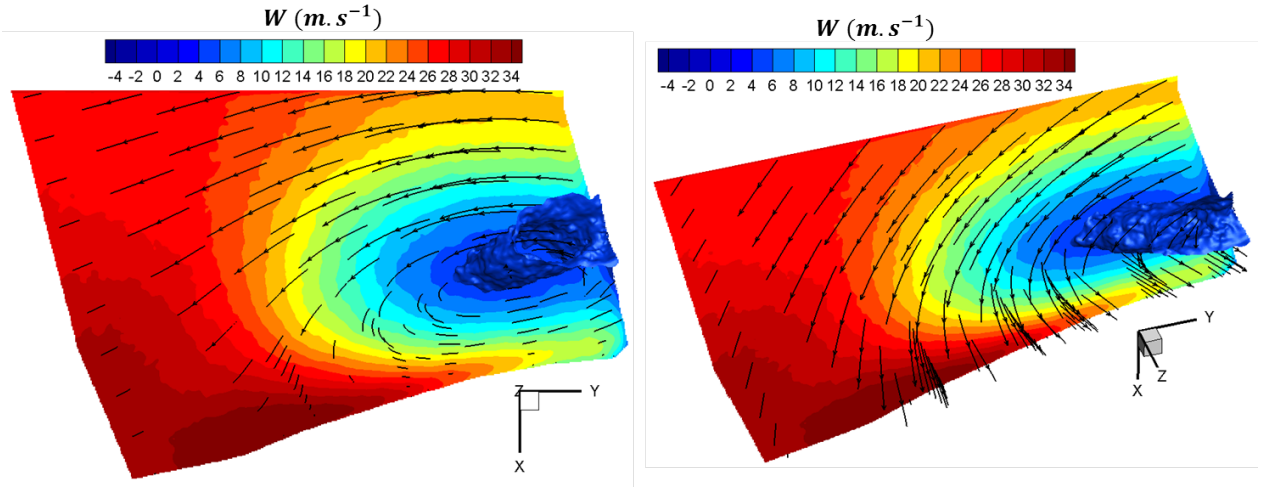

Figure 4: Three-dimensional views (normal to Z axis and perspective) of the mean flow obtained in natural conditions, featuring 3D streamlines and iso-lines of W velocity component in a planar cut at $Z = -5mm$ (most upstream location). 3D Iso-contour $W = 5m.s^{-1}$ has been represented in order to provide an order of magnitude of the vortex core size. Note however that this core is located slightly below the point corresponding to minimum W.

4 Pressure reconstruction results

4.1 Approach and processing parameters

To reconstruct volumic pressure fields from the TomoPIV results, we use the Pressure Schur Complement (PSC) method, exposed in more detail in our companion paper by Carini et al. We consider here the steady Reynolds-Averaged Navier-Stokes equations:

$$\begin{aligned} (u \cdot \nabla) u - \nu \nabla^2 u + \nabla p &= -\nabla \cdot \langle u' \otimes u' \rangle \quad \text{and} \quad \nabla \cdot u = 0 \quad \text{on} \, \Omega, \\ u|_{\partial\Omega} &= b, \end{aligned} \tag{1}$$

rewritten into the following Stokes problem:

$$\begin{aligned} -\nabla^2 v + \nabla \tilde{p} &= g \quad \text{and} \quad \nabla \cdot v = 0 \quad \text{on} \, \Omega, \\ v|_{\partial\Omega} &= b \end{aligned} \tag{2}$$

upon introducing the notations $\tilde{p} = p/\nu$ and $v = u$. Boundary conditions b and source term $g = -\frac{1}{\nu}\left[(u \cdot \nabla) u + \nabla \cdot \langle u' \otimes u' \rangle\right]$ are obtained from the experimental velocity fields. In this problem, only $\tilde{p}$ is kept, v acting as a dummy variable. The specificity, and one of the advantages of this method, is thus that the pressure problem can be solved by prescribing Dirichlet boundary conditions on the domain *on the velocity*, which is the directly

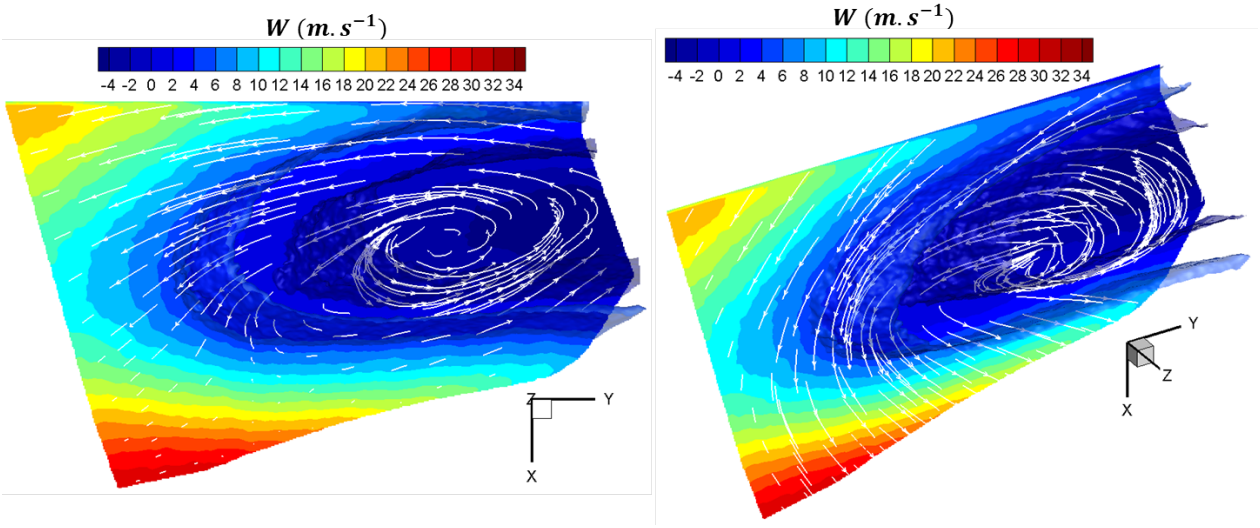

Figure 5: Three-dimensional views (normal to Z axis and perspective) of the mean flow obtained with LE blowing on, featuring 3D streamlines and iso-lines of W velocity component in a planar cut at $Z = -5mm$ (most upstream location). 3D Iso-contour $W = 0$ and $5m.s^{-1}$ have been represented in order to provide an order of magnitude of the vortex core size. Note however that this core is located slightly below the point corresponding to minimum W.

measured quantity. Also, Stokes problem (2) is quite classical in computational fluid dynamics so that efficient existing parallelized routines can be used to tackle it. Here, a finite-element discretisation of the velocity and pressure fields, so that problem (2) reduces to a linear system of the form:

$$\begin{bmatrix} L_u & \tilde{G} \\ G^T & 0 \end{bmatrix} \begin{pmatrix} v \\ \tilde{p} \end{pmatrix} = \begin{pmatrix} g \\ 0 \end{pmatrix}, \tag{3}$$

which is solved using a Schur complement method, yielding the volumic pressure field.

4.2 Results

Volumic pressure computation using the PSC method has been performed on both runs. In practice, for each case this led to solving a $58,378,737 \times 58,378,737$ system, which was run on 840 cores, and required up to 1.05 TB of memory. Figures 8 and 9 show results of these reconstruction in the $Z = 0$ plane, coinciding with the wall pressure tap generatrix. Each figure shows the contours of pressure coefficient $C_p = 2(p - p_\infty)/\rho U_\infty$ in the whole plane, and compares values closest to the wall yielded by PSC with values measured by the taps. In the case of PSC, no particular tap was used as a reference for the absolute pressure level. Instead, it was preferred to choose this reference value so that the integral above both C_p curves (PSC and pressure taps) coincide, in order not to favor a particular sensor.

In the natural case, the PSC method appears to capture truthfully the signature of the leading edge vortex, which is characterized by a strong depression at the location of the vortex core. The pressure profile extracted closest to the wing's upper surface compares well with the pressure tap measurements (cf. Fig. 8, right) along almost the whole profile, for $-0.16 \leq y \leq -0.10$. Closest to the vortex core, for $y \geq -0.8$, reconstructed C_p however deviates from the pressure tap measurements. This is probably ascribed to the fact that, due to remaining light reflection, the lower edge of the reconstructed volume does not exactly coincide with the wall, but is rather located a few mm above. As is well known in aerodynamics and pressure from PIV, curved streamlines (as in the case of a vortex) are associated with a pressure gradient normal to the curvature, so that here, extrapolation of pressure directly below a vortex core can be particularly error-prone.

In the case with leading edge blowing however, the pressure field and pressure profile above the wing yielded by PSC appear very flat, with almost no gradient. Although this can be consistent with the presence of vortex breakdown, which consists in a large stagnation zone with strongly reduced rotation velocities (therefore decreasing the magnitude of the associated pressure drop), it does not compare well with the

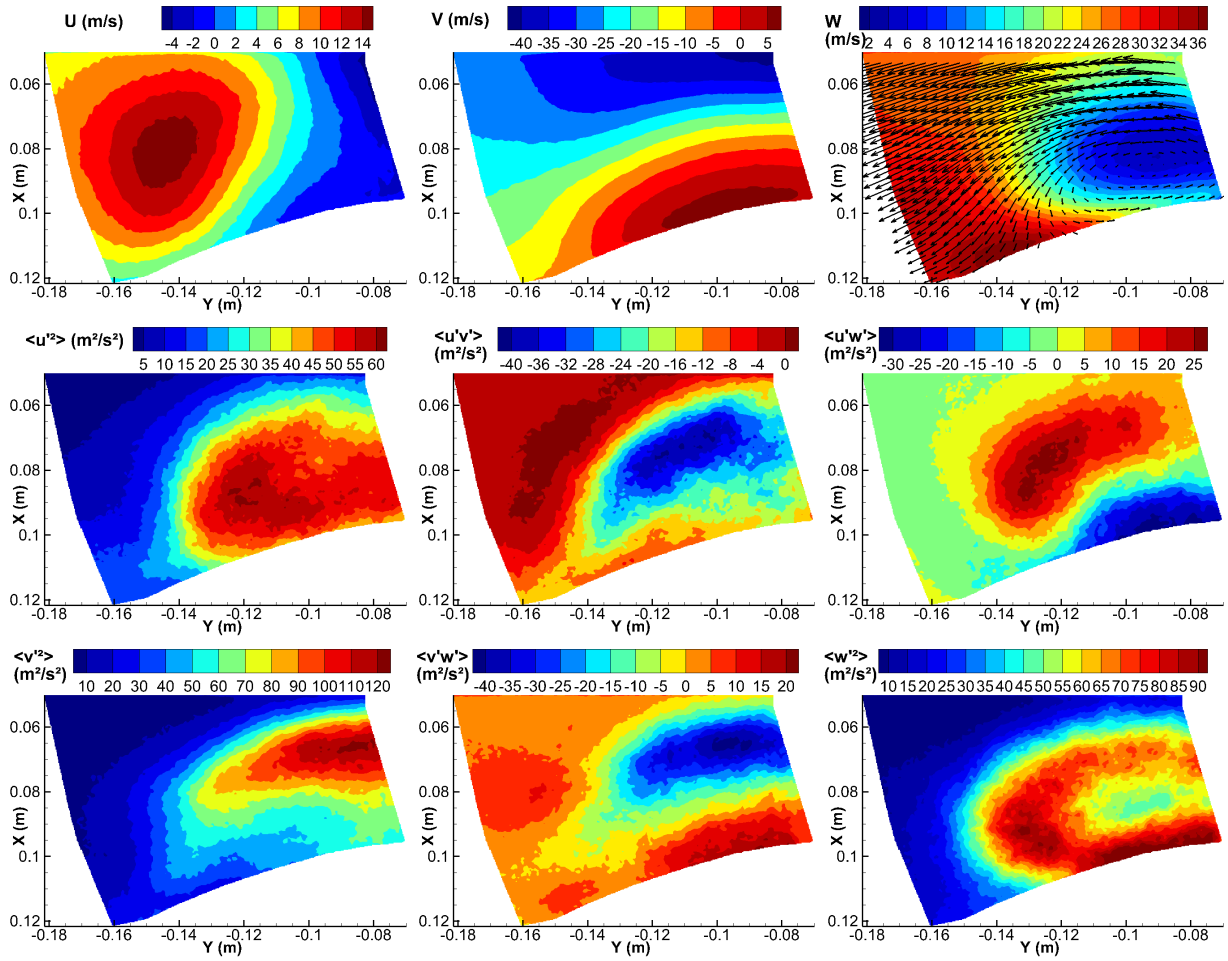

Figure 6: Iso contours of mean flow (top row) and Reynolds stresses (middle and bottom rows) in slice $Z = 0$ corresponding to the location of the pressure tap generatrix, natural case.

pressure taps. Indeed, these still record a pressure drop as Y decreases, although of lesser magnitude than in the natural case. As a first hypothesis, one could think of the influence of the Reynolds stresses, and of their partial convergence due to a limited number of samples. Indeed, as described in section 3.2, this flow situation with vortex breakdown is characterized by a much higher turbulence rate than the natural case (compare for instance subfigures for $\langle u'^2 \rangle$, $\langle v'^2 \rangle$ and $\langle w'^2 \rangle$ in Figures 6 and 7). However, monitoring of convergence in the flow did not show a substantial difference in the statistical uncertainty between both runs. Besides, to further assess this hypothesis, we also performed a reconstruction in this case with blowing, by neglecting the Reynolds stresses, and found a very similar result, confirming that their influence was not significant. Consequently, in the same spirit as what has been observed in the natural case for $y \geq -0.8$, we hypothesize that this discrepancy should be most probably ascribed to the fact that, here again, the lowest velocity and therefore pressure information is only a few millimetres above the model wall. Note that, this could be all the more true as, during this run, a more intense light reflection than in the natural case was observed, as a result of a slight change in the light sheet settings, leading to a larger gap from the wall in the results. Upon comparing Figures 6 and 7, a current hypothesis is that, due to breakdown, a zone of higher rotational velocity than that observed in the velocity fields might be located in the inaccessible band close to the wall, leading to a pressure drop and therefore explaining the values recorded by the pressure taps. A hint possibly supporting this hypothesis is the spatial structure of $\langle w'^2 \rangle$ in both cases, suggesting that in the case with leading edge blowing on, a band of high values of this quantity might be located in the inaccessible zone, together with a high vortical activity. Further works will thus aim at investigating possibilities of more optimized processings allowing to obtain information even closer to the wall.

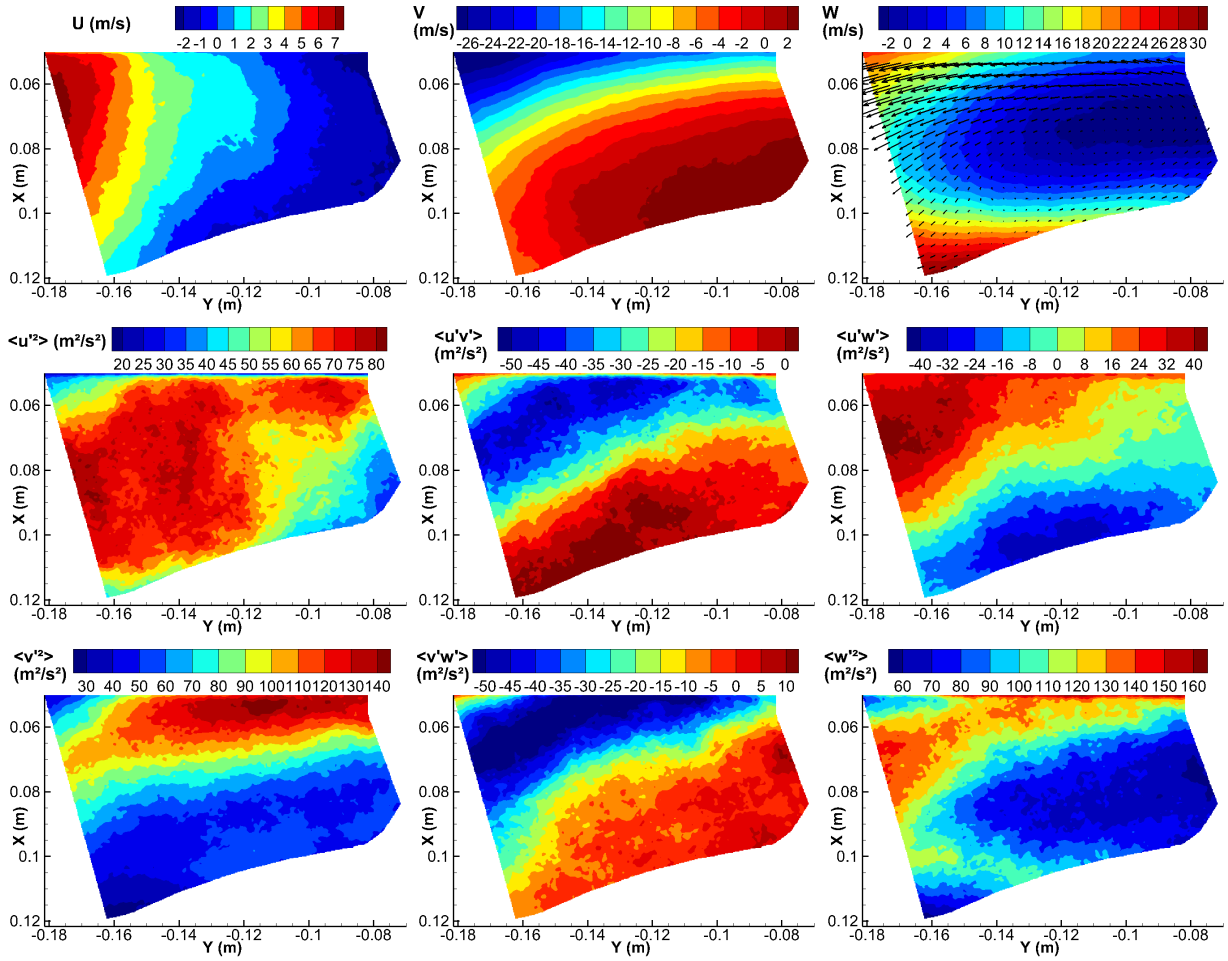

Figure 7: Iso contours of mean flow (top row) and Reynolds stresses (middle and bottom rows) in slice $Z = 0$ corresponding to the location of the pressure tap generatrix, leading edge blowing on. Vectors in the top right figure as the same scale as in Figure 6.

5 Conclusion

A campaign of tomographic PIV measurements has been performed in a flow zone over the upper surface over a flying wing model set at 20^o angle of attack, at chord Reynolds number equal to $1.1\,10^{-6}$, with the final aim to experimentally assess the accuracy of a newly introduced pressure reconstruction method, the Pressure Schur Complement (described in our companion paper Carini et al.). To do so, the volumic illumination has been placed so as to embed a generatrix of wall pressure taps, providing a reference for the reconstruction. Angle-of-attack has been chosen to promote a strong wingtip vortex in the natural case, while leading edge blowing has been used to provoke highly different flow conditions without any geometrical change. Tomographic PIV results have indeed confirmed the presence of a strong vortex in the natural case, undergoing breakdown when leading edge blowing was activated. Both cases were observed to be strongly turbulent, with highest levels for the latter. Pressure reconstructions with PSC were performed in the two situations. While a very good agreement with the pressure taps was found in the natural situations, except for the taps located directly below the vortex core, reconstructed pressures in the case with leading edge blowing were very different from the pressure taps profiles. While confirming the performance of PSC in a difficult experimental context (large wind tunnel and test section dimensions, self-calibration for each individual snapshot), discrepancies have been ascribed to the existence of a gap between the lowest accessible value of velocity in the laser volume, and thus of pressure, and the model, in zones with a possibly high downwards pressure gradient (curved streamlines). Future steps will thus aim at optimizing even more the near wall processings. However, as light reflections often set a strong constraint on the results, the extent of these

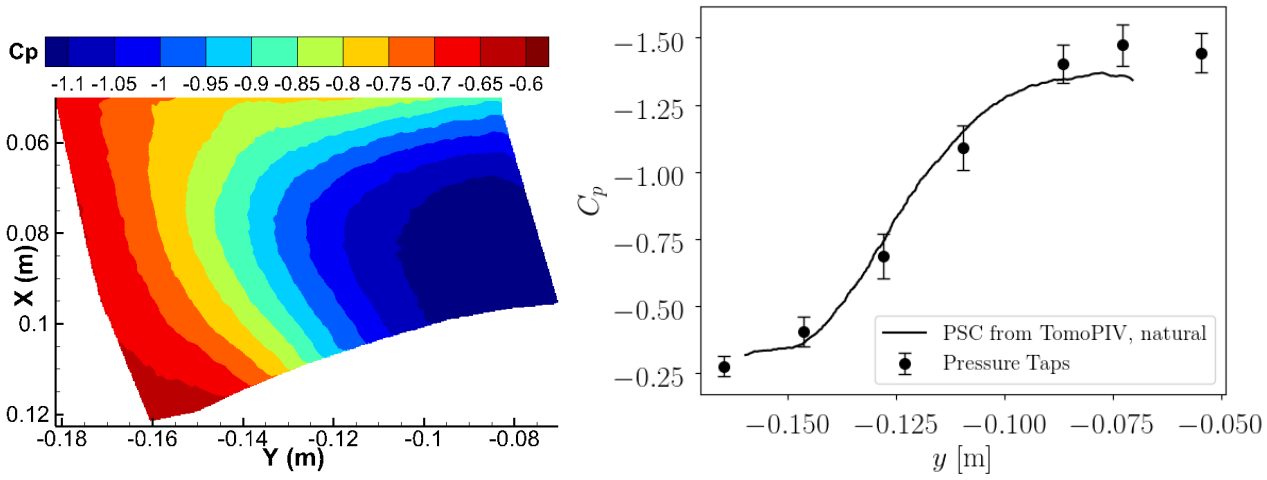

Figure 8: Results of PSC pressure reconstruction from TomoPIV, natural case. Left: C_p contours in the plane containing pressure taps. Right: Comparison between the pressure taps and reconstructed pressure extracted along the line at the bottom edge of the domain (larger values of X for each abscissa Y).

improvements could be limited, so that different post-processing steps such as data assimilation, known to be able to reconstructed information in gaps, might be another promising option.

The authors acknowledge the financial support of the Agence Nationale pour la Recherche and the DGA under the grant ANR-16-ASTR-0005-01, as well as the CPER-FEDER of the Hauts-de-France region.

References

Atkinson C and Soria J (2009) An efficient simultaneous reconstruction technique for tomographic particle image velocimetry. *Experiments in Fluids* 47:553

Cheminet A, Leclaire B, Champagnat F, Plyer A, Yegavian R, and Le Besnerais G (2014) Accuracy assessment of a lucas-kanade based correlation method for 3d piv. in *17th International Symposium on Applications of Laser Techniques to Fluid Mechanics*

Cornic P, Illoul C, Cheminet A, Le Besnerais G, Champagnat F, Le Sant Y, and Leclaire B (2016) Another look at volume self-calibration: calibration and self-calibration within a pinhole model of scheimpflug cameras. *Measurement Science and Technology* 27:094004

Jentzsch MP, Taubert L, and Wygnanski IJ (2016) Active flow control on the stability and control configuration (saccon). in *8th AIAA Flow Control Conference*. page 3168

Le Roy JF, Morgand S, and Farcy D (2014) Static and dynamic derivatives on generic ucav without and with leading edge control. in *32nd AIAA Applied Aerodynamics Conference*. page 2391

Schütte A, Hummel D, and Hitzel SM (2012) Flow physics analyses of a generic unmanned combat aerial vehicle configuration. *Journal of Aircraft* 49:1638–1651

Tormalm M, Le Roy JF, and Morgand S (2016) Numerical assessment of leading-and trailing-edge control on a swept lambda wing. *Journal of Aircraft* 55:603–622

Van Gent P, Michaelis D, Van Oudheusden B, Weiss PÉ, de Kat R, Laskari A, Jeon YJ, David L, Schanz D, Huhn F et al. (2017) Comparative assessment of pressure field reconstructions from particle image velocimetry measurements and lagrangian particle tracking. *Experiments in Fluids* 58:33

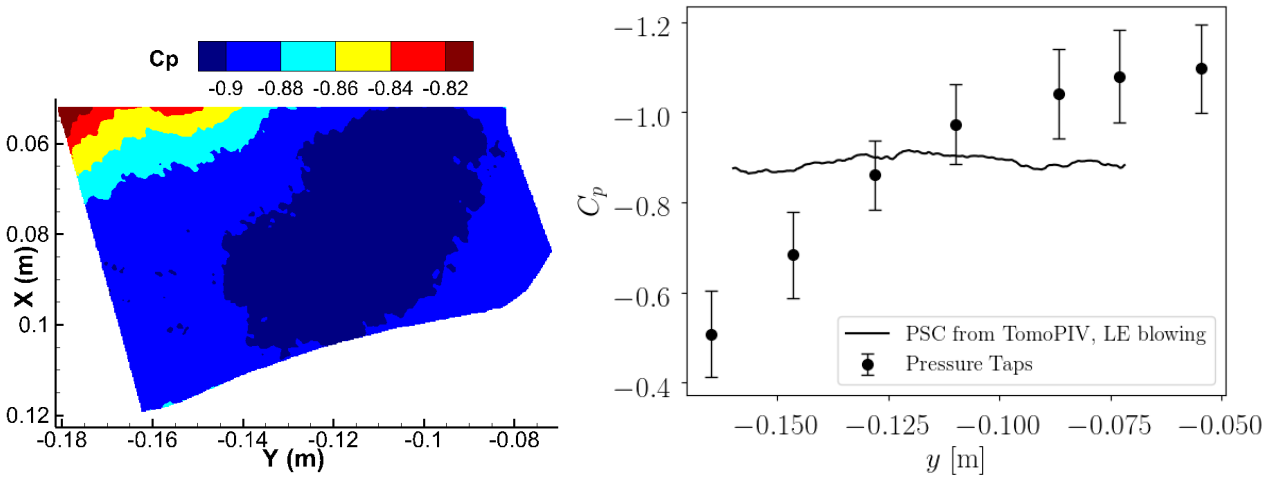

Figure 9: Results of PSC pressure reconstruction from TomoPIV, with leading-edge blowing on. Left: C_p contours in the plane containing pressure taps. Right: Comparison between the pressure taps and reconstructed pressure extracted along the line at the bottom edge of the domain (larger values of X for each abscissa Y).